



Since January 2020 Elsevier has created a COVID-19 resource centre with free information in English and Mandarin on the novel coronavirus COVID-19. The COVID-19 resource centre is hosted on Elsevier Connect, the company's public news and information website.

Elsevier hereby grants permission to make all its COVID-19-related research that is available on the COVID-19 resource centre - including this research content - immediately available in PubMed Central and other publicly funded repositories, such as the WHO COVID database with rights for unrestricted research re-use and analyses in any form or by any means with acknowledgement of the original source. These permissions are granted for free by Elsevier for as long as the COVID-19 resource centre remains active.



Synthesis, biological evaluation and molecular modeling of a novel series of fused 1,2,3-triazoles as potential anti-coronavirus agents

Konstantina Karypidou^a, Sergio R. Ribone^b, Mario A. Quevedo^b, Leentje Persoons^c, Christophe Pannecouque^c, Christine Helsen^d, Frank Claessens^d, Wim Dehaen^{a,*}

^a Molecular Design and Synthesis, Department of Chemistry, KU Leuven, Celestijnenlaan 200F, 3001 Leuven, Belgium

^b Unidad de Investigación y Desarrollo en Tecnología Farmacéutica (UNITEFA, CONICET), Dpto. Farmacia, Fac. Ciencias Químicas, Universidad Nacional de Córdoba, Córdoba X5000HUA, Argentina

^c Department of Microbiology and Immunology, Laboratory of Virology and Chemotherapy, Rega Institute for Medical Research, KU Leuven, Herestraat 49, B-3000 Leuven, Belgium

^d Laboratory of Molecular Endocrinology, Department of Cellular and Molecular Medicine, KU Leuven, Herestraat 49, B-3000 Leuven, Belgium

ARTICLE INFO

Keywords:

Respiratory syndrome
Coronavirus
3CL protease
1,2,3-triazole
Biological evaluation

ABSTRACT

Synthesis and biological evaluation of a novel library of fused 1,2,3-triazole derivatives are described. The in-house developed multicomponent reaction based on commercially available starting materials was applied and broad biological screening against various viruses was performed, showing promising antiviral properties for compounds **14d**, **14n**, **14q**, **18f** and **18i** against human coronavirus 229E. Further *in silico* studies identified the key molecular interactions between those compounds and the 3-chymotrypsin-like protease, which is essential to the intracellular replication of the virus, supporting the hypothesis that the protease is the target molecule of the potential antiviral derivatives.

Coronaviruses are single-stranded RNA viruses associated with mild to severe respiratory symptoms. Human coronaviruses (HCoV) strains HCoV-229E and HCoV-OC43 were first described in the 1960s as causes for respiratory tract infections in humans, including common cold and pneumonia.¹ In 2002–2003, a new human coronavirus, named SARS-CoV, was identified as the etiological agent for the global outbreak of severe acute respiratory syndrome (SARS), which caused the death of over 800 individuals among 8000 cases worldwide, representing a fatality rate of almost 10%.^{2–4} Since then three additional coronaviruses have been recognized. Initially, HCoV-NL63⁵ and HCoV-HKU1,⁶ were reported causing acute respiratory diseases of lower severity compared to the SARS-CoV and more recently, Middle East respiratory syndrome (MERS-CoV) causing lethal respiratory diseases.^{7,8} To date, there are no approved antiviral drugs or vaccines available for the prevention and/or treatment of SARS-like viruses making the development of effective antiviral agents an imperative need.⁹

Coronaviruses express two proteases, a papain-like protease (PL^{PRO}) and a 3-chymotrypsin-like protease (3CL^{PRO}). The 3CL^{PRO} enzyme, also referred to as Main protease (M^{PRO}), is essential to the intracellular viral replication, making it an attractive target for the development of novel

inhibitors.¹⁰ Reports in the literature classify potential antiviral compounds into two main categories: i) the peptidomimetics (Fig. 1A) and ii) small molecule-based inhibitors (Fig. 1B) presenting both activities in μM and nM range. Despite the satisfying initial results, the majority of those promising compounds did not proceed to clinical studies due to nonideal physicochemical properties.⁹

References on non-peptidic inhibitors accentuate the presence of the benzotriazole group. The importance of this benzotriazole motif relies on the formation of key interactions with the catalytic dyad, Cys145 and His41, of the 3CL^{PRO} active site.¹¹ Considering our interest in the chemistry of 1,2,3-triazole bioactive molecules and their interesting binding mode, we wanted to prepare a novel library of fused 1,2,3-triazoles and subsequently determine their biological activity.

Here, we reported our preliminary results on the development of a novel series of fused 1,2,3-triazole compounds and their potential antiviral activity. For this purpose, we implemented the multicomponent reaction developed within our group, which resulted in a plethora of 1,2,3-triazole derivatives in a single step starting from readily available enolizable carbonyl compounds, primary amines and 4-nitrophenyl azide. In general, the method proceeds *via* an equilibrium of imine/

* Corresponding author.

E-mail addresses: konstantina.karypidou@kuleuven.be (K. Karypidou), sribone@fcq.unc.edu.ar (S.R. Ribone), alfredoq@fcq.unc.edu.ar (M.A. Quevedo), leentje.persoons@kuleuven.be (L. Persoons), christophe.pannecouque@kuleuven.be (C. Pannecouque), christine.helsen@kuleuven.be (C. Helsen), frank.claessens@kuleuven.be (F. Claessens), wim.dehaen@kuleuven.be (W. Dehaen).

<https://doi.org/10.1016/j.bmcl.2018.09.019>

Received 25 July 2018; Received in revised form 11 September 2018; Accepted 15 September 2018

Available online 22 September 2018

0960-894X/© 2018 Elsevier Ltd. All rights reserved.

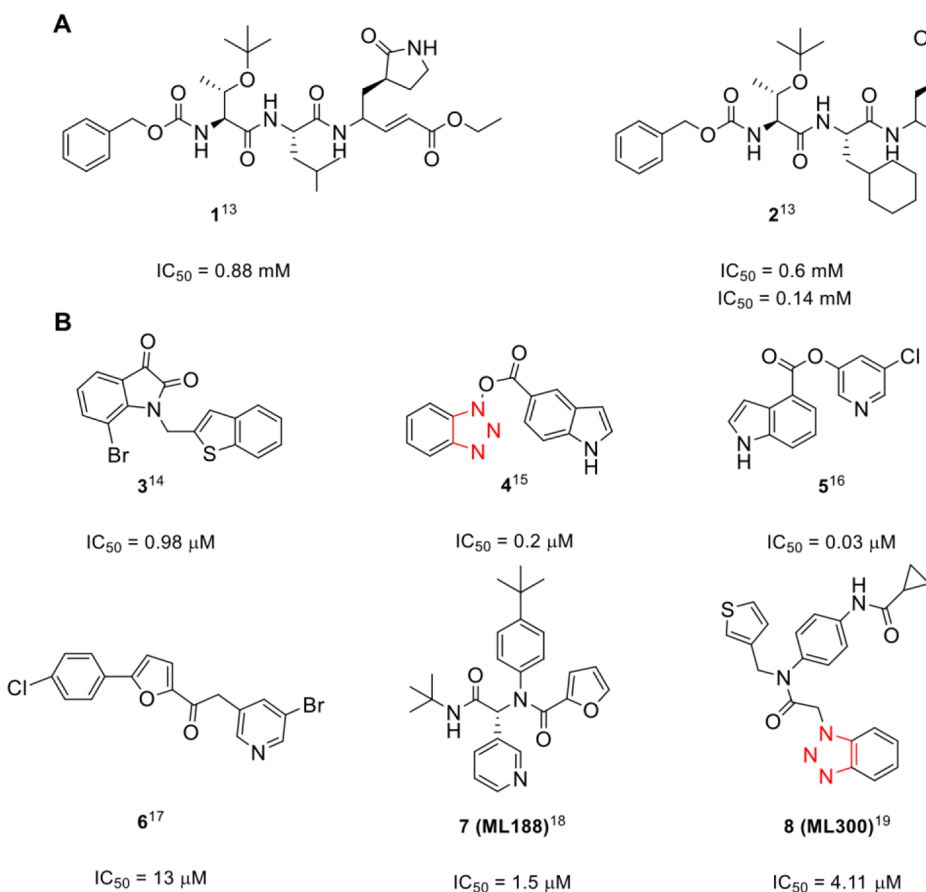


Fig. 1. Representative A) peptidic¹³ and B) small molecule SARS-CoV 3CL^{pro} inhibitors.^{14–19}

enamine followed by [3 + 2] cycloaddition with the azide.¹² This leads to a triazolone intermediate which after elimination of 4-nitroaniline results in the final fused 1,2,3-triazole analogues.

The synthesis, presented in Scheme 1, began by following a general method to generate the oxopiperidine carboxylate intermediate which involves Michael addition of aniline onto ethyl acrylate followed by an intramolecular Dieckmann condensation.²⁰ Subsequent nucleophilic substitution with benzyl bromide provided the starting material **11** in 65% overall yield. Once **11** was obtained, we proceeded for the fused triazole formation using a collection of primary amines and 4-nitrophenyl azide (PNA, **13**).

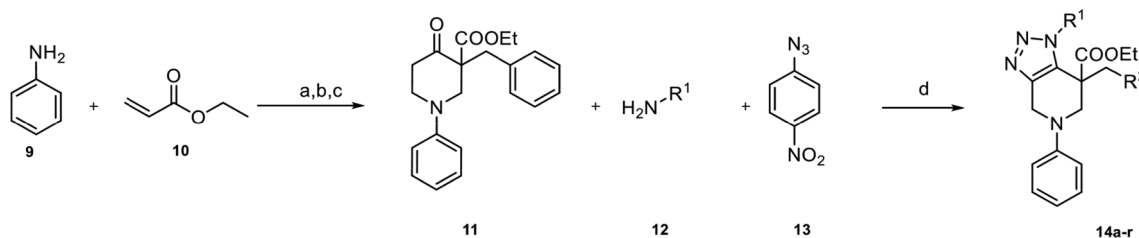
We commenced our investigations with benzylic amines bearing both electron-donating functional groups, (Table 114b, c) and electron-withdrawing groups, (Table 114d–j). Both families were obtained in moderate to good yields.

Further analysis using heterocyclic and aliphatic derivatives **14k–p** proved the applicability of these substituents under the high temperature conditions used in this reaction (Table 1). Furthermore, we examined the influence of the introduction of a fluoro group on the benzyl

bromide on the reactivity (Table 1, entries 17 and 18), which demonstrated that there is no effect on the outcome of the reaction.

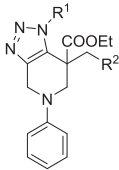
A second series of fused 1,2,3-triazole analogues was prepared based on the previously described multicomponent method, starting from *N*-phenyl-4-piperidone material **17** which in turn was synthesized according to Buchwald-Hartwig Pd-catalyzed amination of different aryl bromides, presented in Scheme 2.²¹ We initially examined the scope of this reaction with respect to primary amines. As we would expect based on the aforementioned results, we managed to synthesize an adequate number of examples in good to excellent yields (**18a–d**). Furthermore, the presence of electron withdrawing substituents on the aryl bromides was explored (**18e–l**). The results are summarized in Table 2.

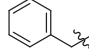
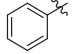
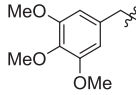
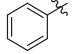
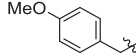
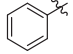
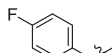
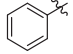
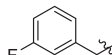
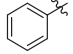
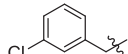
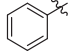
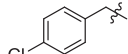
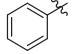
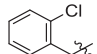
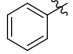
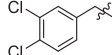
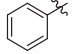
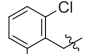
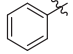
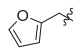
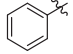
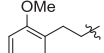
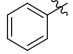
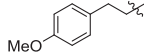
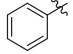
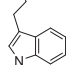
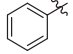
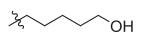
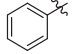
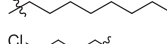
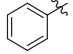
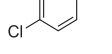
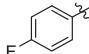
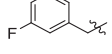
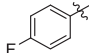
The compounds were evaluated against a broad variety of viruses including HIV-1 (strain III_B), HIV-2 (strain ROD) in MT-4 cells, herpes simplex virus type 1 (strain KOS), herpes simplex virus type 2 (strain G), herpes simplex virus type 1 TK⁻ (KOS) ACV^{res}, vaccinia virus, adeno virus-2 and coronavirus (229E) in HEL cells and their inhibitory activity was compared to that of reference compounds as zidovudine, brivudine,



Scheme 1. Synthetic pathway towards derivatives **14a–r**. Reagents and conditions: (a) AcOH, CuCl, 24 h, 110 °C, 55%, (b) NaH, Toluene, EtOH, 6 h, 100 °C, 90%, (c) BnBr, K₂CO₃, THF, 6 h, 70 °C, 65%, (d) Toluene, 18 h, 100 °C.

Table 1
Molecular structures, yield and biological activity against coronavirus (229E) of derivatives **14a–r**.



Entry	Compound ID	R ¹	R ²	Yield	EC ₅₀ (μM) ^a
1	14a			80%	> 100
2	14b			85%	> 100
3	14c			65%	> 100
4	14d			80%	8.95
5	14e			58%	> 100
6	14f			80%	> 100
7	14g			67%	> 100
8	14h			48%	> 100
9	14i			30%	> 100
10	14j			73%	> 100
11	14k			55%	> 100
12	14l			56%	> 100
13	14m			85%	> 100
14	14n			80%	9.45
15	14o			57%	> 100
16	14p			51%	> 100
17	14q			50%	9.45
18	14r			60%	> 100

^a Concentration required to reduce virus-induced cytopathogenicity by 50%.

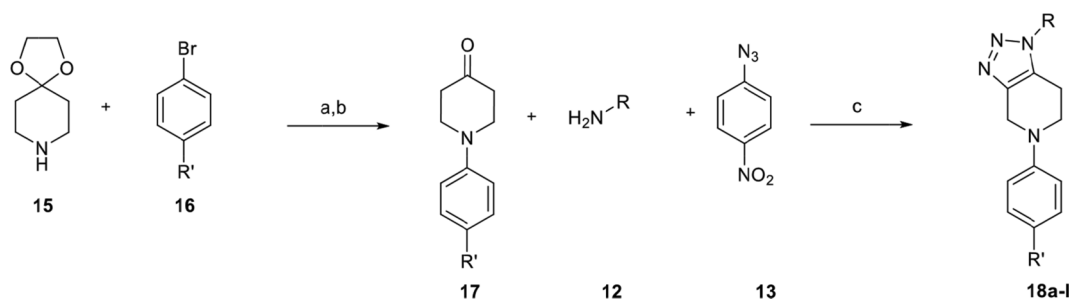
cidofovir, acyclovir, ganciclovir, zalcitabine, alovudine and *Urtica dioica* agglutinin (UDA), respectively. All compounds were inactive towards all tested viruses, while **14d** (EC₅₀ = 8.95 μM), **14n**

(EC₅₀ = 9.45 μM), **14q** (EC₅₀ = 9.45 μM), **18f** (EC₅₀ = 8.90 μM) and **18i** (EC₅₀ = 11.95 μM) showed moderate activity against human coronavirus (229E), but all approximately 50 fold lower than the activity observed with UDA (EC₅₀ = 0.2 μM). No alterations of the normal cell morphology in confluent HEL cell cultures was observed at concentrations up to 100 μM (data not shown). The selectivity index (SI) (MCC/EC₅₀ ratio) was > 8 for all active compounds.

To determine the structure-activity relationship (SAR) for the synthesized library of fused 1,2,3-triazoles, it is of utmost importance to identify the key intermolecular contacts involved in the non-covalent interaction between 3CL^{pro} and the structurally diverse inhibitors. With this aim, several molecular modeling techniques, including molecular docking, molecular dynamics, free energy of binding analyses and intermolecular interaction scanning, were applied in the search of such SAR knowledge. In a first stage, previously reported 3CL^{pro} non-covalent inhibitors were modeled in order to define the key intermolecular interactions required for enzyme inhibition, while in a second stage the *in silico* analysis was extended to the family of fused 1,2,3-triazoles presented in this report.

The catalytic activity of 3CL^{pro} has been well characterized, with extensive details regarding the structure of this enzyme and the corresponding catalytic site. In this respect, it is known that the active site is located within domains I and II, in which a catalytic dyad consisting of residues Cys145 and His41 is located.¹¹ It has also been previously reported that the catalytic site of 3CL^{pro} exhibits a stereoselective recognition of non-covalent inhibitors.¹⁸ In this context, our molecular modeling protocols initiated with the exploration of the binding mode, intermolecular interaction pattern and stereoselectivity of the non-covalent inhibitor of 3CL^{pro} deposited in the Protein Databank under the code 3V3M. Both enantiomers of the bound ligand were docked within the catalytic site, and as can be seen in Fig S1a,b, the *R* enantiomer resulted in an identical interaction pattern to that observed in the experimentally obtained crystal. The ligand binding is stabilized by several hydrophobic and hydrogen bond (HB) interaction, of which those with Glu166, His163 and Gly143 are of particular relevance. Noteworthy, the *S* enantiomer was also able to establish several hydrophobic interactions, but was not able to establish HB with Glu166 and His163. Taking into account that it has been previously reported that only the *R* enantiomer is active,¹⁸ this finding suggests that the establishment of interactions with Glu166 and His163 constitutes a critical feature to inhibit the catalytic activity of the enzyme. To further study the persistence of these HB interactions, the intermolecular complexes were subjected to molecular dynamics (MD) analysis, with Table S1 presenting the persistence value (%) for each HB as calculated from the MD trajectories. As can be seen in Table S1, entry 1, the *R* enantiomer was able to maintain in relatively high frequencies the HB interactions with Glu166, His163 and Gly143, while the *S* enantiomer rearranged its binding to contact only Glu166 (60% persistence). Our findings not only validate the molecular modeling workflow we developed (i.e. the crystallographic binding pose was reproduced), but also strongly suggests that at least two stable electrostatic interactions within the active site are required for effective 3CL^{pro} inhibition.²¹

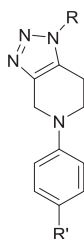
To further study this hypothesis, a set of 12 previously reported 3CL^{pro} inhibitors containing a fused 1,2,3 triazole ring and exhibiting a wide range of inhibitory activities (i.e. between 51 and 26000 nM, Tables S3 and S5), was subjected to our molecular modeling workflow. The lowest energy binding mode obtained for TS8 was in agreement with the reported crystallographic structure (Fig. S3d and pdb code 4MDS, respectively), further supporting an adequate parametrization and simulation conditions of the molecular modeling protocol. From inspection of the corresponding lowest energy docked poses for the whole set of compounds (Figs. S2–S4), we observed that all these inhibitors were indeed able to establish the two HB previously described for 3V3M, i.e. one with the backbone of Glu166 and another one with the side chain of His163. In these binding modes, the triazole ring is positioned in the proximity of the catalytic dyad. From the MD



Scheme 2. Reagents and conditions: (a) Pd(OAc)₂, XPhos, NaO-*t*-Bu, Toluene/*t*-BuOH (5:1), 18 h, 120 °C, 65%, (b) aq. HCl (5 N), 3 h, 100 °C, 45%, (c) Toluene, 18 h, 100 °C.

Table 2

Molecular structures, yield and biological activity against coronavirus (229E) of derivatives **18a–l**.



Entry	Compound ID	R	R'	Yield	EC ₅₀ (μM) ^a
1	18a		H	85%	> 100
2	18b		H	74%	> 100
3	18c		H	90%	> 100
4	18d		H	48%	> 100
5	18e		-CF ₃	90%	> 100
6	18f		H	85%	8.9
7	18g		H	85%	> 100
8	18h		H	89%	> 100
9	18i		H	85%	11.95
10	18j		H	89%	> 100
11	18k		-F	91%	> 100
12	18l		H	57%	> 100

^a Concentration required to reduce virus-induced cytopathogenicity by 50%.

simulations and the quantification of the persistence of the above mentioned hydrogen bond interactions (Table S1, entries 3–14), we observed that all the compounds maintained the hydrogen bonds required for the inhibition of 3CL^{pro} in high frequencies, and in particular

that with Glu166. It is noteworthy that inhibitors that are enantiomerically pure and exhibiting submicromolar activities maintained high frequencies of HB with Glu166 and His163. In particular, TS-1, which is by far the most potent compound within the training set, exhibited also a single cluster of docked poses, suggesting not only an efficient pharmacodynamic interaction with 3CL^{pro}, but also an adequate conformational preorganization that is compliant with the corresponding bioactive conformation.

Compounds **14a–r** and **18a–l** were subjected to the molecular modeling workflows in order to study whether 3CL^{pro} may represent a plausible molecular target for their observed antiviral activity. Figs. S5 and S9 shows the lowest energy binding modes to 3CL^{pro} found for compounds **14a–r**. When the docked poses corresponding to the bioactive derivatives are observed (i.e. **14d** and **14n**, Figs. S5d, S8b, respectively), it can be seen that they establish the two HB interactions with Glu166 and His163, positioning also the triazole ring in the proximities of the catalytic dyad. As it was discussed in previous sections, this interaction pattern is required for the inhibition of 3CL^{pro} catalytic activity, suggesting that this enzyme may be the antiviral target of these fused 1,2,3-triazoles. Further analysis by MD also showed that these interactions are maintained throughout the simulation, further supporting their bioactivities (Table S2, entries 4, 14 and 17). In contrast, the fused triazole derivatives that did not exhibited antiviral activities in infected cells, did not establish these two HB interactions in the lowest energy binding pose, or were not able to form them during the simulation trajectory when subjected to MD assays. Compounds **14c** and **14m** constitute two exceptions to this behavior, both of them bearing a methoxy substituent on the para position of the phenyl ring substituting the triazole central scaffold. These two compounds were able to establish and maintain the HB interaction pattern required for 3CL^{pro} inhibition, (Table S2, entries 3 and 13) but did not exhibit antiviral activity. This fact may be due to a disfavorable entropic contribution upon binding to the 3CL^{pro} catalytic site, since in order to maintain the interaction with His163, the rotation of the methoxy group is constrained within a dihedral angle of 10 Å. Clearly, this entropic cost is not present for the bioactive analogue bearing a fluorine atom in the para position (**14d**).

When derivatives **18a–l** were analyzed (Figs. S10–S12), a similar behavior was observed, with the derivatives exhibiting antiviral activity (i.e. **18f** and **18i**) being able to establish two stable HB interactions within the catalytic site of 3CL^{pro} (Figs. S11b and S12a). In particular, derivative **18f** is anchored within the catalytic site through a stable interaction with His163, with two additional interactions being established with Glu166 and Thr25. Regarding the interaction of **18i**, this compound establishes stable HB contacts with both Glu166 and His163, while further anchoring to residue Gln189. As a result, both compounds positioned the fused triazole scaffold in the vicinity of the catalytic dyad which is consistent with blocking the protease activity of the enzyme. Finally, when the interaction patterns of the inactive compounds within the series **18a–l** were analyzed, we found that all of them failed to establish the two required HB interactions within the catalytic site of the enzyme.

In conclusion, we have succeeded in synthesizing a novel library of fused 1,2,3-triazoles using the in-house developed multicomponent reaction. The library was subjected to *in vitro* analysis using a broad variety of viruses to determine their antiviral properties and to *in silico* studies to determine the interactions with 3CL^{pro}. Compounds **14d**, **14n**, **14q**, **18f** and **18i** showed moderate activity against coronavirus 229E. A molecular modeling work flow was developed based on previously reported 3CL^{pro} non-covalent inhibitors and helped the identification of key molecular interactions. Application of this model to our library, supports that the antiviral activity is mediated through the inhibition of 3CL^{pro}. Additional studies on the structure-activity relationship will enable us to prepare new fused 1,2,3-triazole derivatives with enhanced antiviral properties.

Acknowledgments

This work was supported by Katholieke Universiteit Leuven (KU Leuven), grants C32/15/033 and ISPLA2/15/03. In addition, the authors gratefully acknowledge financial support from the Secretaria de Ciencia y Técnica of the Universidad Nacional de Córdoba (SECYT-UNC), the Consejo Nacional de Investigaciones Científicas y Técnicas (CONICET), and the Agencia Nacional de Promoción Científica y Técnica (ANPCyT). The authors would also like to thank the GPGPU Computing Group from the Facultad de Matemática, Astronomía y Física (FAMAF), Universidad Nacional de Córdoba, Argentina, for providing access to computing resources. The authors also gratefully acknowledge the support of NVIDIA Corporation with the donation of the Titan Xp GPU used for this research. Mario A. Quevedo wishes to thank OpenEye Scientific Software and their Free Academic Licensing program for providing him with licenses to use the corresponding software packages.

Appendix A. Supplementary data

Supplementary data to this article can be found online at <https://doi.org/10.1016/j.bmcl.2018.09.019>.

References

- Bradburne AF, Bynoe ML, Tyrrell DAJ. Effects of a "New" human respiratory virus in volunteers. *Br Med J*. 1967;3:767–769.
- Drosten C, Günther S, Preiser W, et al. Identification of a novel coronavirus in patients with severe acute respiratory syndrome. *N Engl J Med*. 2003;348:1967–1976. <https://doi.org/10.1056/NEJMoa030747>.
- Kuiken T, Fouchier RAM, Schutten M, et al. Newly discovered coronavirus as the primary cause of severe acute respiratory syndrome. *Lancet*. 2003;362:263–270. [https://doi.org/10.1016/S0140-6736\(03\)13967-0](https://doi.org/10.1016/S0140-6736(03)13967-0).
- Communicable Disease Surveillance and response; WHO. SARS case fatality ratio, incubation period. http://www.who.int/csr/sars/archive/2003_05_07a/en/.
- Published 7 May 2003.
- Van Der Hoek L, Pyrc K, Jebbink MF, et al. Identification of a new human coronavirus. *Nat Med*. 2004;10:368–373. <https://doi.org/10.1038/nm1024>.
- Woo PCY, Lau SKP, Chu C, et al. Characterization and complete genome sequence of a novel coronavirus, coronavirus HKU1, from patients with pneumonia. *J Virol*. 2005;79:884–895. <https://doi.org/10.1128/JVI.79.2.884-895.2005>.
- Zaki AM, Van Boheemen S, Bestebroer TM, Osterhaus ADME, Fouchier RAM. Isolation of a novel coronavirus from a man with pneumonia in Saudi Arabia. *N Engl J Med*. 2012;367:1814–1820. <https://doi.org/10.1056/NEJMoa1211721>.
- Chan JFW, Lau SKP, To KKW, Cheng VCC, Woo PCY, Yuen KY. Middle East Respiratory syndrome coronavirus: another zoonotic betacoronavirus causing SARS-like disease. *Clin Microbiol Rev*. 2015;28:465–522. <https://doi.org/10.1128/CMR.00102-14>.
- Zumla A, Chan JFW, Azhar EI, Hui DSC, Yuen KY. Coronaviruses-drug discovery and therapeutic options. *Nat Rev Drug Discov*. 2016;15:327–347. <https://doi.org/10.1038/nrd.2015.37>.
- Pillaiyar T, Manickam M, Namasivayam V, Hayashi Y, Jung SH. An overview of severe acute respiratory syndrome-coronavirus (SARS-CoV) 3CL protease inhibitors: peptidomimetics and small molecule chemotherapy. *J Med Chem*. 2016;59:6595–6628. <https://doi.org/10.1021/acs.jmedchem.5b01461>.
- Anand K, Ziebuhr J, Wadhwani P, Mesters JR, Hilgenfeld R. Coronavirus main proteinase (3CL pro) structure : basis for design of anti-SARS drugs. *Science*. 2003;300:1763–1767. <https://doi.org/10.1126/science.1085658>.
- Thomas J, Jana S, John J, Liekens S, Dehaen W. A general metal-free route towards the synthesis of 1,2,3-triazoles from readily available primary amines and ketones. *Chem Commun*. 2016;52:2885–2888. <https://doi.org/10.1039/c5cc08347h>.
- Yang S, Chen SJ, Hsu MF, Wu JD, Tseng CTK, Liu YF, Chen HC, Kuo CW, Wu CS, Chang LW, Chen WC, Liao SY, Chang TY, Hung HH, Shr HL, Liu CY, Huang YA, Chang LY, Hsu JC, Peters CJ, Wang AHJ, Hsu MC. Synthesis, crystal structure, structure-activity relationships, and antiviral activity of a potent SARS coronavirus 3CL protease inhibitor. *J Med Chem*. 2006;49:4971–4980. <https://doi.org/10.1021/jm0603926>.
- Chen LR, Wang YC, Lin YW, et al. Synthesis and evaluation of isatin derivatives as effective SARS coronavirus 3CL protease inhibitors. *Bioorg Med Chem Lett*. 2005;15:3058–3062. <https://doi.org/10.1016/j.bmcl.2005.04.027>.
- Wu CY, King KY, Kuo CJ, et al. Stable benzotriazole esters as mechanism-based inactivators of the severe acute respiratory syndrome 3CL protease. *Chem Biol*. 2006;13:261–268. <https://doi.org/10.1016/j.chembiol.2005.12.008>.
- Ghosh AK, Gong G, Grum-Tokars V, et al. Design, synthesis and antiviral efficacy of a series of potent chloropyridyl ester-derived SARS-CoV 3CLpro inhibitors. *Bioorg Med Chem Lett*. 2008;18:5684–5688. <https://doi.org/10.1016/j.bmcl.2008.08.082>.
- Zhang J, Huitema C, Niu C, et al. Aryl methylene ketones and fluorinated methylene ketones as reversible inhibitors for severe acute respiratory syndrome (SARS) 3CLike proteinase. *Bioorg Chem*. 2008;36:229–240. <https://doi.org/10.1016/j.bioorg.2008.01.001>.
- Jacobs J, Grum-Tokars V, Zhou Y, et al. Discovery, synthesis, and structure-based optimization of a series of N-(tert-Butyl)-2-(N-arylamido)-2-pyridin-3-yl) acetamides (ML188) as potent noncovalent small molecule inhibitors of the severe acute respiratory syndrome coronavirus (SARS-CoV) 3CLpro. *J Med Chem*. 2013;56:534–546. <https://doi.org/10.1021/jm301580n>.
- Turlington M, Chun A, Tomar S, et al. Discovery of N-(benzo[1,2,3]triazol-1-yl)-N-(benzyl)acetamido)phenyl) carboxamides as severe acute respiratory syndrome coronavirus (SARS-CoV) 3CLpro inhibitors: identification of ML300 and noncovalent nanomolar inhibitors with an induced-fit binding. *Bioorg Med Chem Lett*. 2013;23:6172–6177. <https://doi.org/10.1016/j.bmcl.2013.08.112>.
- Gallagher MJ, Mann FG. The structure and properties of certain polycyclic indolo- and quinolinoderivatives. Part XV. Derivatives of 1-phenyl-4-piperidone and its phosphorus and arsenic analogues. *J Chem Soc*. 1962;23:5110.
- Schön U, Messinger J, Buckendahl M, Prabhu MS, Konda A. An improved synthesis of N-aryl and Nheteroaryl substituted piperidones. *Tetrahedron Lett*. 2007;48:2519–2525. <https://doi.org/10.1016/j.tetlet.2007.02.053>.